Fractional model of the chemical inductor

Enrique Hernández-Balaguera

Escuela Superior de Ciencias Experimentales y Tecnología (ESCET), Universidad Rey Juan Carlos, 28933 Móstoles, Madrid, Spain

ARTICLE INFO

ABSTRACT

A multitude of materials and processes of a different nature frequently exhibit, in addition to the classical capacitive arcs, inductive loops in the complex impedance plane. It is a stable and physically robust response originated, from a mathematical perspective, by the introduction of a capacitive coupling in the slow relaxation variable. Nevertheless, the dynamical behavior of such systems shows, in reality, pronounced experimental deviations from the ideal inductive behavior. For this reason, the scientific community in general claims for the development of a novel theory that helps to phenomenologically interpret this pattern change, also encompassing the associated inherent physical complexity that capitalizes on the vast majority of real-world processes. Here, we present a generalization of the classical fast-slow models to naturally explain the anomalous dynamics observed experimentally in different types of measurement techniques, such as the inductance dispersion in impedance, the fractional relaxation processes with negative spike components in the transient responses, and the inverted current-voltage hysteresis. From numerical simulations, we analyze in detail the crossover dynamics from capacitive to inductive properties from the perspective of the constant phase element. Our work devises a useful theoretical framework that explains, in frequency and time domain, the coexistence of dispersive features and the transformation of the electrical behavior in terms of an anomalous bifractional crossover. Finally, we show the dominant role of the fractional-order dynamics in the appearance of inverted hysteresis commonly found in current-voltage curves. Although in literature, everything looks, in a certain manner, simple, the reality is that many real-world materials exhibit an intricate and complex nature that leads to anomalous processes evidenced by dispersive dynamics observed through different measurement techniques. This change of pattern analyzed here is appealing as a mathematical tool to interpret the physical phenomena of many familiar systems.

1. Introduction

The fundamental operating principles of an inductor, based on electromagnetic phenomena, can be traced to Michael Faraday. Based on the concept of magnetic field, Faraday's law explains the physics behind this basic passive element, based on the idea that the induction of voltage in a current-carrying conductor is a consequence of the lines of force surrounding it. Conceptually, the inductor is a two-terminal element that opposes any change in electrical current. Its physical arrangement consists of a coil of fine wire wrapped around a supporting core of commonly magnetic material. Inductance, symbolized by L and measured in henrys (H), is the circuit parameter used to describe an inductor [1]. Assuming the passive sign convention and linear time-invariant conditions, yields

$$v_L(t) = L \frac{di_L(t)}{dt} \qquad (1)$$

which reflects that reference direction for the variable current $i_L(t)$ is in the direction of the reference voltage drop $v_L(t)$ across the terminals of this familiar element. Note that a "linear time-invariant inductor" is a two-terminal component whose flux $\varphi(t)$ and current $i_L(t)$ fall on some fixed curve in the $\varphi - i_L$ plane that does not change with time. Let us consider now that we drive the inductor by an external voltage $v_L(t)$. The corresponding current $i_L(t)$ is obtained by integrating both sides of Eq. (1):

$$i_L(t) = i_L(t_0) + \frac{1}{L} \int_{t_0}^{t} v_L(\tau) \, d\tau \qquad (2)$$

where $i_L(t_0)$ represents the initial value of the current corresponding to the instant t_0 that summarizes the effect of $v_L(\tau)$, from $\tau = -\infty$ to $\tau = t_0$ on the present value of $i_L(t)$. Eq. (2) clearly shows that an inductive current depends on the entire past history (i.e., $t_0 < \tau < t$) of $v_L(\tau)$. Hence, the inductor has "memory" and the best suited way to modeled it

consists of implementing, in parallel with an initially uncharged inductive element, a current source of $i_L(t_0)$ amperes. An important observation is that $i_L(t)$ cannot change by a finite amount in zero time, which gives rise to the inductor current continuity property. The only exception would consist of applying an infinite voltage (Dirac delta function) and thus, the inductor voltage could become unbounded [2].

In the presence of constant current, the inductor current decays exponentially to zero, with such passive circuit element behaving as a short circuit in steady-state conditions. Nevertheless, the systematic application of time-varying signals, specifically sinusoidal excitations, requires the phasor transform in circuit analysis. In an inductor, the relationship between the phasor versions of current and voltage leads to the following impedance function:

$$Z_L(\omega) = \frac{V_L(\omega)}{I_L(\omega)} = j\omega L \tag{3}$$

where j is the imaginary unit and ω is the angular frequency ($\omega = 2\pi f$, where f is frequency). The usual interpretation of the impedance of an inductor is related to the effect of sinusoidal electromagnetic induction, in which a coiled wire linking a time-varying flux magnetic whose lines of force collapse into, or cut, such conductor. In particular, the inductive current lags behind the respective voltage by $\pi/2$. Nevertheless, it exists a wide range of dynamical systems belonging to multiple disciplines that formally, probed in frequency space, produce the same impedance response without the presence of underlying electromagnetic phenomena. In this sense, Bisquert has recently formulated a general denomination, denoted as "chemical inductor" [3], for this class of models showing this anomalous behavior due to slow and delayed ionic effects. In practice, these systems of multidisciplinary applications however do not exhibit ideal inductive responses, requiring the adoption of a constant phase element (CPE), whose impedance function is $Z_{CPE}(\omega) = {}^1/_{Q(j\omega)^\alpha}$ [4], with negative exponents, instead of a pure inductor of chemical origin. Note that Q and α are the parameters defining the CPE. Therefore, there is a need to reexamine this circuit element in order to capture the real information of the electrical behavior of many systems for a given set of experimental conditions.

Although the capacitive version of the CPE is a widely spread electrical element for the analysis of experimental impedance data, only a few works recognize the "inductive face" of this component even though the experimental data show prominent deviations from the ideal pattern. Specifically, the inductance dispersion has been recognized in the fields of electronics and physics; e.g., in supercapacitors [5], memristors [6], and photovoltaic cells [7]. However, it is clear that the ubiquitous depressed semicircles are experimentally present in many materials and processes belonging to different disciplines, such as electrochemistry [8–10], neurosciences [11,12], or materials science [13–15]. Similarly, a wide variety of systems with inductive behavior in frequency space exhibit, at the same time, transient current responses (in response to constant voltage steps) with negative spikes [3,16] and, immediately after, non-linear growths and, at long time scales, monotonically rising forms; i.e., the hallmark of the fractional dynamics [17,18]. For this reason, the impedance of the CPE is commonly given by $Z_\alpha(\omega) = {}^1/_{C_\alpha(j\omega)^\alpha}$, where C_α represents the pseudo-capacitance in units of $F \times s^{\alpha-1}$ ($Q = C_\alpha$) and α, on the other hand, denotes a dimensionless parameter, comprised between 0 and 1, that quantifies the deviation from the ideal pattern. Logically, this ubiquitous element behaves as a pure capacitor, when $\alpha = 1$ [19]. The complex impedance plot, in a Nyquist diagram (Z_r vs. $-Z_j$), of a CPE is a straight line forming an angle of $\alpha\pi/2$ with the Z_r-axis; however, the most common way to visualize the dispersive behavior associated to CPE effects, familiar in many research fields, is in form of arcs (adding resistive effects) more or less depressed depending on the value of α [20–22]. Fig. 1 shows an illustration of impedance diagrams for CPEs obtained for an ideal, electrical parallel-plate capacitor ($\alpha = 1$), for decreasing values of α ($0 < \alpha < 1$)
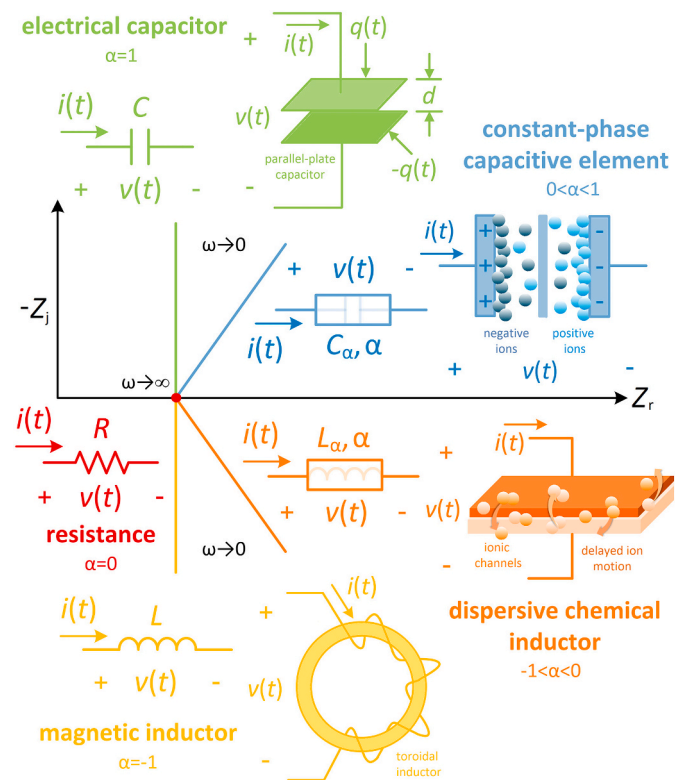

Fig. 1. Complex plane plots of impedance responses for ideal (capacitive $\alpha = 1$, resistive $\alpha = 0$, and inductive $\alpha = -1$) mechanisms and dispersive ($0 < \alpha < 1$ and $-1 < \alpha < 0$) phenomena in terms of the generalized form consisting of the constant phase element (CPE).

connected to multiple trapping processes, and even α crossing the frontier of "negative values". If $\alpha = 0$, the CPE models a resistor whereas when α takes negative values ($-1 < \alpha < 0$), it is appropriate to wonder about the origin of the associated dispersion, associated in principle to ionic time-delayed effects, and rethink its formulation in the form of a constant-phase inductive element. When α belongs to the range from -1 to 0, the shape of the Nyquist plot is significantly modified because theoretically it emerges the formation of straight lines with negative angles, associated to inductive effects with frequency-dependent losses (refer to Fig. 1) or, in real-world systems, flattened semicircles in the fourth quadrant with a dispersive inductor that decreases the resistance [7]. Finally, the classical, magnetic toroidal inductor gives a vertical line ($-\pi/2$ to the real axis) on the complex plane impedance plot when $\alpha = -1$.

Before proceeding any further, it is necessary point out that we define, without loss of generality, $\phi = |\alpha|$ for the sake of convenience in the mathematical treatment, although this does not conform to the standard notation used in the analysis and synthesis of distributed-parameter electrical networks. Rewriting thus the impedance function of the CPE results:

$$Z_\phi(\omega) = L_\phi(j\omega)^\phi, \qquad 0 < \phi \le 1 \tag{4}$$

where L_ϕ is a frequency-independent pseudo-inductance in units of $H/_{s^{1-\phi}}$. If $\phi = 1$, the voltage leads the current by $\pi/2$, and thus, losses now are preferably expressed by $\tan(\theta)$, where θ is the angle that quantifies the deviation from the ideality, $\pi/2$. The full details for a new look at the inductor theory, in the context of the CPE, are given in Appendix A.

In what follows, we report a dynamical framework, based on an engineering type of theory, which leads to anomalous and dispersive inductances, commonly found in a wide variety of practical devices and

systems under experimental conditions. We start off by generalizing the conventional two-dimensional fast-slow model to one case with scale-free memory effects, substituting the integer-order equations by fractional ones. Next, we formulate the dynamical properties in terms of impedance functions, introducing a set of characteristic parameters that completely define the different types of experimental spectra in line with the nature of the internal ionic/electronic processes. Complex impedance responses are exactly given by Cole-Cole forms, normal and inverted, depending on the range of frequency under study. After discussing some basic properties of the fractional framework, we proceed by deriving the corresponding transient relaxation functions of the Mittag-Leffler type with the ubiquitous negative spikes as result of the crossover, from positive to negative, of the fractional operator in the current-voltage relationship. To conclude, we develop, in this sense, numerical simulations with the aim to track the real transition from normal to inverted hysteresis in experimental current-voltage measurements and cyclic voltammetry at different voltage sweeps. The dispersive pattern under interest here is appealing as a theoretical tool to adequately model and determine the physical properties of many natural materials and systems.

2. Model and dynamical properties

2.1. Fundamental basis of the constant-phase inductive element in time-domain

Our model of the chemical inductor is therefore based on the time-domain current-voltage relationship given by a fractional-order derivative:

$$v_\phi(t) = L_\phi \frac{d^\phi i_\phi(t)}{dt^\phi} \tag{5}$$

where $v_\phi(t)$ and $i_\phi(t)$ are the voltage and current of the dissipative chemical inductor. The operator $d^\phi i_\phi(t)/dt^\phi$, according to classical definition of Riemann-Liouville, corresponds to the integro-differential equation:

$$\left[\frac{d^\phi i_\phi(t)}{dt^\phi}\right]_{RL} = \frac{d}{dt}\left\{\frac{t^{-\phi}}{\Gamma(1-\phi)} * i_\phi(t)\right\} = \frac{1}{\Gamma(1-\phi)}\frac{d}{dt}\int_0^t \frac{i_\phi(\tau)}{(t-\tau)^\phi}d\tau, \quad t > 0 \tag{6}$$

which can be interpreted as the first-order derivative of the convolution transform in time of $i_\phi(t)$ with the power-law kernel $t^{-\phi}/\Gamma(1-\phi)$. From the Riemann-Liouville operator of order $-\phi$ (fractional integration or convolution operation of Eq. (6)), it is also possible to estimate the time-domain chemical inductor's current expression:

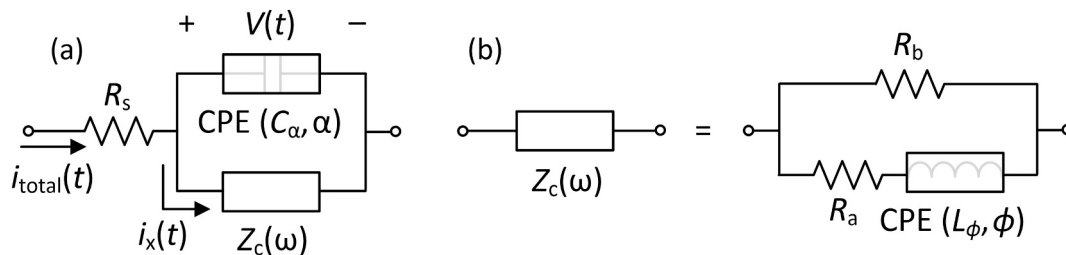$$i_\phi(t) = \frac{1}{L_\phi \Gamma(\phi)}\int_0^t \frac{v_\phi(\tau)}{(t-\tau)^{1-\phi}}d\tau, \quad t > 0 \tag{7}$$

An alternative definition of the fractional derivative is often given, in Caputo sense, as

$$\left[\frac{d^\phi i_\phi(t)}{dt^\phi}\right]_C = \frac{1}{\Gamma(1-\phi)}\int_0^t (t-\tau)^{-\phi}\frac{di_\phi(\tau)}{d\tau}d\tau, \quad t > 0 \tag{8}$$

Both approaches require the use of both a first-order derivative and a fractional-order integration, with the order of the two operations being different [23]. Here arise the famous inequalities that relate the Leibniz rule with the fractional derivatives. The two multistep definitions of the fractional derivative of order ϕ (Eqs. (6) and (8)) are not equivalent to each other and the introduction of a "time-dependent correction term" is indeed necessary [24]:

$$\left[\frac{d^\phi i_\phi(t)}{dt^\phi}\right]_C = \left[\frac{d^\phi i_\phi(t)}{dt^\phi}\right]_{RL} - \frac{t^\phi}{\Gamma(1-\phi)}i_\phi(0) \tag{9}$$

except, logically, in the case of homogeneous initial conditions. In the latter definition, the initial conditions are described in terms of integer-order derivatives, which is not the case in Eq. (7) that weakens the conditions on the function $i_\phi(t)$ and provokes confusion in the physical interpretation. For this reason, the Riemann-Liouville definition is mainly used in the mathematical community and the Caputo one attracts more attention by the researchers in multidisciplinary applications [25].

2.2. General framework of fractional-order two-dimensional dynamical systems

A general electrical description, adaptable to a specific interface and/or process under study, is presented in Fig. 2(a). The circuit representation consists of a resistance R_s in series with the parallel combination of a non-ideal capacitor or CPE with $0 < \alpha < 1$ –see Fig. 1– (e.g., double layer or depletion region) and an impedance, $Z_c(\omega)$ that commonly represents the anomalous effects of the heterogeneous charge-transfer phenomena. For example, $Z_c(\omega)$ can be interpreted as the Faradaic impedance in electrochemical systems, $Z_c(\omega) = Z_F(\omega)$ [26]. In general, $Z_c(\omega)$ is broken down into additional components (see below), where the general dynamical structure of the dispersive chemical inductor, familiar in many research fields, emerges. In effect, a wide variety of systems, including that of biological, electronic, and electrochemical nature, are controlled by similar fundamental phenomena which can be mathematically unified in a general minimal model that contains both a fast-destabilizing and a slow recovery variable [27]. The key here is to accurately describe the slowing down kinetics and long timescale mechanisms that are responsible, to a certain extent, for the occurrence of memory effects in these systems. These features can be described as a function of the potential $V(t)$ and a quantity $X(t)$ which is a characteristic and internal parameter of the system (e.g., the surface concentration in chemical systems, ion channel current in neurons, electron density or current in semiconductors, etc.). Note that multiple examples of the physical meaning of $X(t)$ in a wide variety of systems can be found in [3,27]. Both variables, $V(t)$ and $X(t)$, represent "fast" and

Fig. 2. Schematic representation of the electrical model under study, with (a) R_s, a series resistance, CPE (C_α, α), a dispersive and passive capacitance, and $Z_c(\omega)$, a general impedance associated to slow phenomena. Typically, $Z_c(\omega)$ is broken down into the components shown in (b), where the resistance R_b manifests the instantaneous conduction channel and the series line R_a-CPE (L_ϕ, ϕ) is generated by a slow and delayed current.

"slow" qualities, defining the dynamics of the system through a set of nonlinear differential equations.

Next, we describe the physical basis of the model. As can be seen in Fig. 2(a), the total current flowing through the electrical circuit is divided into the following two components:

$$i_{\text{total}}(t) = C_\alpha \frac{d^\alpha V(t)}{dt^\alpha} + i_{\text{x}}(t) \tag{10}$$

A part of $i_{\text{total}}(t)$ is a fast displacement current that charges the dispersive capacitance –considered later as $i_\alpha(t)$– and the remaining current $i_{\text{x}}(t)$, on the other hand, models the slow relaxation phenomena. It can be expressed, in time-domain, as follows [26]:

$$i_{\text{x}}(t) = f(V(t), X(t)) \tag{11}$$

where the function $f(V(t), X(t))$ represents a combination of conduction currents, each one described by the dependences of the function itself. Furthermore, it is important to point out that this conduction channel is affected by the internal state variable $X(t)$, whose dynamics can be analogously defined by the following fractional-order equation:

$$\frac{d^\phi X(t)}{dt^\phi} = g(X(t), V(t)) \tag{12}$$

causing the memory effects by a voltage-driven adaptable function, $g(X(t), V(t))$ [7].

In effect, this two-dimensional simplified model of physical systems defines the general structure of a fractional-order chemical inductor by using the nonlinear functions $f(V(t), X(t))$ and $g(X(t), V(t))$ that define the dynamical properties of widely different materials. Note that Eqs. (5) and (12) exhibit the same non-integer order ϕ. Although this anomalous effect is however visible in highly nonlinear systems, the linearized equations around a given stationary point contain relevant information about the behavior of the system [28]. For this reason, we next consider a linear stability analysis of Eqs. (11) and (12). The linearized equations, obtained as the response $\Delta i_{\text{x}}(t)$ to a small-amplitude excitation and derived from the first-order Taylor expansion around the steady-state value, are:

$$\Delta i_{\text{x}}(t) = \left(\frac{\partial f}{\partial V}\right)_{\bar{X}} \Delta V(t) + \left(\frac{\partial f}{\partial X}\right)_{\bar{V}} \Delta X(t) \tag{13}$$

$$\frac{d^\phi(\Delta X(t))}{dt^\phi} = \left(\frac{\partial g}{\partial X}\right)_{\bar{V}} \Delta X(t) + \left(\frac{\partial f}{\partial V}\right)_{\bar{X}} \Delta V(t) \tag{14}$$

where $\bar{X}$ and $\bar{V}$ are steady-state values.

For simplicity, we denote the partial derivates as:

$$f'_{\text{V}} = \left(\frac{\partial f}{\partial V}\right)_{\bar{X}}, \quad f'_{\text{X}} = \left(\frac{\partial f}{\partial X}\right)_{\bar{V}} \tag{15}$$

$$g'_{\text{V}} = \left(\frac{\partial g}{\partial V}\right)_{\bar{X}}, \quad g'_{\text{X}} = \left(\frac{\partial g}{\partial X}\right)_{\bar{V}} \tag{16}$$

In this scenario, the introduction of Laplace transforms methods in the small perturbations Eqs. (13) and (14), $d/dt \to s$ and $s = j\omega$, yields the following transfer functions:

$$\frac{\widetilde{i_{\text{x}}}}{\widetilde{V}} = f'_{\text{V}} + f'_{\text{X}} \frac{\widetilde{X}}{\widetilde{V}} \tag{17}$$

$$\frac{\widetilde{X}}{\widetilde{V}} = \frac{g'_{\text{V}}}{(j\omega)^\phi - g'_{\text{X}}} \tag{18}$$

Substituting Eq. (18) into Eq. (17) and with some algebraic manipulations, we obtain the form of the dispersive impedance:

$$Z_{\text{c}}(\omega) = \left[f'_{\text{V}} + f'_{\text{X}} \frac{g'_{\text{V}}}{(j\omega)^\phi - g'_{\text{X}}}\right]^{-1} \tag{19}$$

Next, we will represent the system by a small ac impedance equivalent circuit.

2.3. Electrical equivalent circuit and classification of impedance spectra

In terms of equivalent circuit elements, the first term of Eq. (19) can clearly be recognized as a resistor:

$$R_{\text{b}} = \frac{1}{f'_{\text{V}}} \tag{20}$$

that accounts, e.g., in electrochemistry, the kinetics of the electron exchange reaction when $i_{\text{x}}(t)$ models the Faradaic current $i_{\text{F}}(t)$ and thus, R_{b} is a charge-transfer resistance, $R_{\text{ct}} = \left(\frac{\partial V}{\partial i_{\text{F}}}\right)_{\bar{V}}$ [26]. Thus,

$$\lim_{\omega \to \infty} Z_{\text{c}}(\omega) = R_{\text{b}} \tag{21}$$

The second one represents an impedance component that is dependent on the signs of the partial derivates f'_{X}, g'_{V}, and g'_{X}. From an introductory inspection of this term, derived from Eq. (18), we firstly see that such complex function will be stable only if $g'_{\text{X}} < 0$; that is, if the single pole lies in the left half of the $j\omega$-plane [28,29]. Note that the characteristic frequency, also known as the inverse of the relaxation time,

$$\omega_{\text{L}} = \frac{1}{\tau_{\text{L}}} = (-g'_{\text{X}})^{1/\phi} \tag{22}$$

represents the negative pole of the impedance transfer function of Eq. (18). Otherwise, Eq. (19) would not obey one of the conditions of the Kramers-Kronig relations (unrestrained response) and therefore it would not model an impedance function in equilibrium conditions. It is important to complete the exploration of the stability properties, for a broader study, through a transient analysis since, according to this perspective, we can observe if the system indeed returns to equilibrium only if the partial derivative g'_{X} is negative. For example, if the applied signal is a voltage step at time $t = 0$, i.e., $\Delta V(t) = |\Delta V|u(t)$ (here $u(t)$ is the standard Heaviside function), the analytical solution of the fractional differential equation of Eq. (14) then is

$$\Delta X(t) = -\frac{g'_{\text{V}}}{g'_{\text{X}}} |\Delta V| (1 - E_\phi[g'_{\text{X}} t^\phi]) \tag{23}$$

where the temporal evolution of the internal variable $X(t)$ that governs this anomalous physical response, operating by small perturbation over a steady-state, is given by the one-parameter Mittag-Leffler function, provided as:

$$E_\phi[g'_{\text{X}} t^\phi] = \sum_{k=0}^{\infty} \frac{[g'_{\text{X}} t^\phi]^k}{\Gamma(\phi k + 1)}, \quad \phi > 0 \tag{24}$$

Following the simplification $\phi = 1$, we obtain the commonly known expression in an ideal stability analysis [26,28]:

$$\Delta X(t) = -\frac{g'_{\text{V}}}{g'_{\text{X}}} |\Delta V| (1 - exp[g'_{\text{X}} t]) \tag{25}$$

where the sign of g'_{X} takes the same general critical restrictions in time-resolved measurements than in frequency-domain for the dynamical properties in terms of instability and oscillations.

Next consider the second term on the right-side of Eq. (19) when $g'_{\text{X}} < 0$. Indeed, the sign of the product $f'_{\text{X}} g'_{\text{V}}$ determines the shape of the low-frequency features [26]. Using different combinations in the sign of the partial derivatives, a variety of qualitatively different spectra can be generated as shown in Fig. 3. For the parameter $f'_{\text{X}} g'_{\text{V}}$ varying from
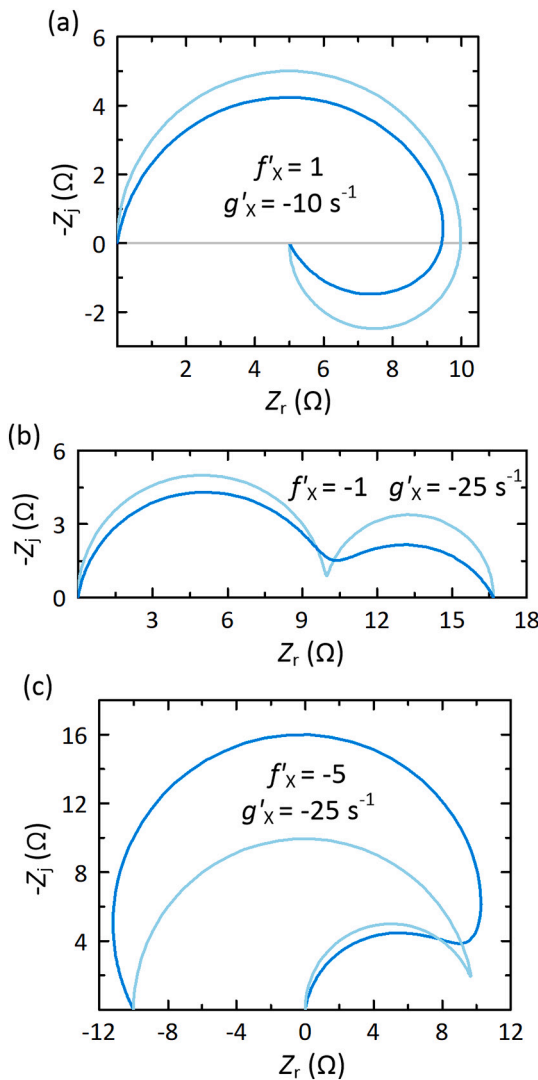
Fig. 3. Complex plane impedance representation of the spectral patterns corresponding to the impedance model shown in Fig. 2, with $R_s = 0\ \Omega$, $C_\alpha = 20\ \mu\text{F cm}^{-2}\ \text{s}^{\alpha-1}$, $f'_V = 0.1\ \Omega^{-1}$, $g'_V = 1$, $\alpha = 1$ and $\phi = 1$ or $\alpha = 0.9$ and $\phi = 0.7$ for sky blue and dark blue lines, respectively, under conditions that satisfy the stability criterion $g'_X < 0$: (a) $f'_X = 1$ and $g'_X = -10\ \text{s}^{-1}$; (b) $f'_X = -1$ and $g'_X = -25\ \text{s}^{-1}$; (c) $f'_X = -5$ and $g'_X = -25\ \text{s}^{-1}$.

positive to negative, we obtain the characteristic low-frequency hooks in the fourth quadrant of the complex plane associated to the chemical inductive effects (a), a classical double arc structure (b), and a negative dc resistance with two semicircles when the inductor becomes negative (c), by considering normal ($\alpha = 1$ and $\phi = 1$) and anomalous ($0 < \alpha < 1$ and $0 < \phi < 1$) processes. All the spectra in Fig. 3 correspond to representative combinations of the characteristic parameters ($f'_X g'_V$ and g'_X). Nevertheless, additional features, such as single positive arcs, hidden negative resistance spectra or hook features close to Hopf bifurcations can emerge in different dynamical regimes of the systems [27], operating in a manner analogous, in the comparison of ideal and dispersive impedance data, to those shown in the paper. Remember that this model reproduces the main experimental characteristics of impedance responses observed and reported by many authors in electrochemistry [9,30], neurosciences [11,12], and semiconductor devices [14,31]. Specifically, the impedance function takes the form:

$$Z_c(\omega) = \left[\frac{1}{R_b} + \frac{1}{L_\phi(j\omega)^\phi + R_a}\right]^{-1} \tag{26}$$

where

$$R_a = -\frac{g'_X}{f'_X g'_V} \tag{27}$$

$$L_\phi = \frac{1}{f'_X g'_V} \tag{28}$$

and thus, there is a basic equivalent circuit, shown in Fig. 2(b), that accounts all the two semicircles.

If $f'_X g'_V > 0$, the values of R_a and L_ϕ are positive and therefore, the two arcs would be one in the positive imaginary half-plane and the other one in the lower half of the complex plane (see Fig. 3(a)). The difference in nature and magnitude between both Nyquist plots shown in Fig. 3(a) can be clearly observed from the resulting spectra. The ideal relaxation pattern is increasingly compressed vertically for decreasing values of α and ϕ because, at sufficiently high and low frequencies, both the real and the imaginary parts of the impedance ($Z_r(\omega)$ and $Z_j(\omega)$) approximately scale like $\omega^{-\alpha}$ and $\omega^{-\phi}$, and their ratios, $Z_j(\omega)/Z_r(\omega)$, are given through $tan(\alpha\pi/2)$ and $tan(\phi\pi/2)$, respectively [18]. They are independent of ω, in contrast to normal relaxation modes, where the ratio is given by $\omega\tau$. This inductive pattern was introduced in neuroscience by Cole and Baker [11].

To clarify the concept of the fractional-order chemical inductor and the associated complex patterns in the impedance spectra when R_a and L_ϕ are positive, let us rewrite the general impedance function of the circuit of Fig. 2(a) but, for the sake of clarity, considering $\alpha = 1$ ($C_\alpha = C$):

$$Z(\omega) = R_s + \frac{Z_c(\omega)}{1 + j\omega C Z_c(\omega)} = R_s + \left[j\omega C + f'_V + f'_X \frac{g'_V}{(j\omega)^\phi - g'_X}\right]^{-1} \tag{29}$$

and the low-frequency limit of the associated admittance, neglecting the series resistance

$$Y(\omega) = f'_V - \frac{f'_X g'_V}{g'_X} - j\omega\left[\frac{f'_X g'_V}{g'^2_X}\frac{sin(\phi\pi/2)}{\omega^{1-\phi}} - C\right], \quad \omega \to 0 \tag{30}$$

which allow us to easily visualize that the depressed low-frequency arc can be interpreted as the composition of a total dc resistance:

$$R_{dc} = \lim_{\omega \to 0} Z_c(\omega) = \left(f'_V - \frac{f'_X g'_V}{g'_X}\right)^{-1} = \left(\frac{1}{R_b} + \frac{1}{R_a}\right)^{-1} \tag{31}$$

and a variable reactance that depends on the sign of $f'_X g'_V$. From Eq. (30) and by considering $f'_X g'_V > 0$, it is possible to establish that the inductive branch becomes "active" when the following condition is satisfied

$$\frac{f'_X g'_V}{g'^2_X} > \frac{C\omega_{ref}^{1-\phi}}{sin(\phi\pi/2)} \tag{32}$$

or if ω is smaller than the frequency associated to the pseudo-resonance operation mode

$$\omega_c = \left[g'_X cos\left(\frac{\phi\pi}{2}\right) - g'_X\sqrt{cos^2\left(\frac{\phi\pi}{2}\right) + \frac{f'_X g'_V}{Cg'^2_X}\frac{sin(\phi\pi/2)}{\omega_{ref}^{1-\phi}} - 1}\right]^{1/\phi} \tag{33}$$

of the circuit shown in Fig. 2(a). Note that ω_{ref} represents an approximation of the frequency reference value, which, from our experience in modeling of systems, the inductive effects commonly emerge. If the constraint of Eq. (32) is not satisfied, only a single positive and depressed arc would be visible in the impedance results [7,14].

In contrast, the impedance response with a double resistive-capacitive arc, whose associated Nyquist diagram is shown in Fig. 3 (b), is obtained when $f'_X g'_V < 0$. Note that we assume, for the moment, a fixed value of g'_X. Both R_a and L_ϕ become negative, but this regime with the characteristic frequency remaining still positive $\omega_L = \left(R_a / L_\phi\right)^{1/\phi}$, does not introduce instabilities [28]. In this sense, an electrical transformation can be introduced to model the slow response of systems. Now, the "heart" of the equivalent circuit could be composed, if one considers positive elements, by two couples of R-CPE elements in matryoshka configuration. We now obtain that the dispersive impedance is equivalent to a Randles circuit given by $Z_c(\omega) = R_b + \left[C_\gamma (j\omega)^\gamma + 1/R_x\right]^{-1}$, where C_γ and γ $(0 < \gamma < 1)$ are the non-ideal capacitance parameter and the dispersion coefficient, respectively, of the new CPE [32]. In effect, the equivalent circuit of $Z_c(\omega)$ could alternatively contain a resistance R_b in series with the parallel combination of a fractional-order capacitor and other resistor, defined, respectively, by Eq. (20) and the following expressions:

$$C_\gamma = -\frac{f'^2_V}{f'_X g'_V} \tag{34}$$

$$R_x = -\frac{f'_X g'_V}{f'_V \left(f'_X g'_V - g'_X f'_V\right)} \tag{35}$$

Before proceeding any further, it is necessary to indicate that

$f'_X g'_V$ and g'_X (R_a and L_ϕ) are the same as in the diagrams of Fig. 3(b) [27,28]. This negative dc resistance spectrum allows us to obtain the stability condition of the general impedance response, provided by the pole, or the characteristic time constant, of the impedance transfer function of Eq. (19):

$$\omega_X = \frac{1}{\tau_X} = \left(\frac{f'_X}{f'_V} g'_V - g'_X\right)^{1/\phi} \tag{36}$$

resulting in the differential condition, with respect to case (b):

$$g'_X < \frac{f'_X}{f'_V} g'_V \tag{37}$$

which, in principle, seems to be less restrictive than the previously indicated constraint, $g'_X < 0$, that prevents an exponential explosion in the state variable $\Delta X(t)$. Note that a similar result can be found under the condition that R_{dc} is positive (see Eq. (31)). In the case (b), $g'_X < f'_X g'_V / f'_V$, and thus, impedance does not cross the imaginary axis and the total resistance is positive. An important point to note is that, in comparison to the ideal semicircular shape corresponding to the exponential patterns, here the dispersive dynamics exhibits higher reactance values associated to the slow characteristic frequency region. The condition of intercept with the vertical axis is $Z_r(\omega) = 0$ and thus, the resulting frequency, by considering for simplicity $\alpha = 1$, is

$$\omega_d = \left[\frac{\omega_L^\phi}{2\omega_b}\left(-(\omega_a + 2\omega_b)cos\left(\frac{\phi\pi}{2}\right) + \sqrt{\left[(\omega_a + 2\omega_b)cos\left(\frac{\phi\pi}{2}\right)\right]^2 - 4\omega_b(\omega_a + \omega_b)}\right)\right]^{1/\phi} \tag{38}$$

impedance description of a multitude of materials and processes undergoes, over a broad range of voltage, a phenomenon of transformation from capacitive to inductive behavior (i.e., a transition from the spectra of Fig. 3(b) to (a) as the voltage bias increases). The dispersive chemical inductor is not real and thus it is possible to emulate it via basic concepts of circuit theory. For instance, the introduction of an active gyrator-capacitor element [33] is coherent in this scenario as it allows to emulate the fractional-order inductive dynamics, in a more elaborate fashion, for real-world systems without electromagnetic effects. This two-port network, composed fundamentally of cross-coupled voltage-controlled current sources, is capable of turning the classical non-ideal capacitor, physically present in many systems, into a dispersive inductor of chemical origin [34]. Indeed, the apparently high values of L_ϕ, usually obtained under experimental conditions, in general are not related to any inductive feature in the sense of an establishment of considerable magnetic fields. Instead, it is possible that they are a natural consequence of a relatively high "gyrative resistance r" when changing voltage: $L_\phi = r^2 C_\gamma$. This methodology offers an alternative, straightforward, and logical way of understanding the dual behavior commonly observed in many materials and systems, in particular when the experimental impedance data do not satisfy the Kramers-Kronig (KK) relations [35].

Inspection of the Fig. 3(b) reveals the following key observations. The impedance spectra, at high frequencies, simply replicate or mirror those of Fig. 3(a). Close to the transition, the frequency response develops, for the fractional dynamics case, a smoother decay in reactance than that of the ideal case, becoming a double arc, with analogous features, at sufficiently low frequencies.

In Fig. 3(c), R_{dc} interestingly crosses the origin, from positive to negative resistance values, at zero frequency even though the signs of

where

$$\omega_a = \left(-\frac{f'_X g'_V}{C_\alpha g'_X}\right)^{1/\alpha} = \left(\frac{1}{R_a C_\alpha}\right)^{1/\alpha} \tag{39}$$

$$\omega_b = \left(\frac{f'_V}{C_\alpha}\right)^{1/\alpha} = \left(\frac{1}{R_b C_\alpha}\right)^{1/\alpha} \tag{40}$$

Indeed, ω_d is real when there is interception of the imaginary axis. Note that Eq. (38) can be simplified to [27]:

$$\omega_d = \omega_L \sqrt{\frac{\omega_a}{\omega_b} - 1}, \quad \phi = 1 \tag{41}$$

when one considers the ideal low-frequency case, $\phi = 1$. Finally, it is necessary to clarify why the imaginary part of the impedance $Z_j(\omega)$ for $0 < \phi < 1$ exhibits a higher value than that of the case of $\phi = 1$ at low frequencies, when $Z_r(\omega) = 0$. In the low frequency region of the complex plane impedance plot, the real part

$$Z_r(\omega) = \frac{1}{f'_X g'_V - g'_X f'_V} \frac{\omega^\phi cos\left(\frac{\phi\pi}{2}\right)\left[1 - g'_X \tau_X^\phi\right] - g'_X + \omega^{2\phi}\tau_X^\phi}{1 + 2(\omega\tau_X)^\phi cos\left(\frac{\phi\pi}{2}\right) + (\omega\tau_X)^{2\phi}} \tag{42}$$

and the imaginary part

$$Z_j(\omega) = \frac{1}{f'_X g'_V - g'_X f'_V} \frac{\omega^\phi sin\left(\frac{\phi\pi}{2}\right)\left[1 + g'_X \tau_X^\phi\right]}{1 + 2(\omega\tau_X)^\phi cos\left(\frac{\phi\pi}{2}\right) + (\omega\tau_X)^{2\phi}} \tag{43}$$

of the dispersive impedance, both connected through the Kramers-Kronig relation, govern and explain the shape of the response. Interestingly, the value of both terms at the characteristic frequency ω_X

E. Hernández-Balaguera

Chaos, Solitons and Fractals: the interdisciplinary journal of Nonlinear Science, and Nonequilibrium and Complex Phenomena 172 (2023) 113470

$$Z_r(\omega_X) = \frac{1}{f'_X g'_V - g'_X f'_V} \frac{\omega_X^\phi cos\left(\frac{\phi\pi}{2}\right)\left[1 - g'_X \tau_X^\phi\right] - g'_X + \omega_X^\phi}{2\left[1 + cos\left(\frac{\phi\pi}{2}\right)\right]} \tag{44}$$

$$Z_j(\omega_X) = \frac{1}{f'_X g'_V - g'_X f'_V} \frac{\omega_X^\phi sin\left(\frac{\phi\pi}{2}\right)\left[1 + g'_X \tau_X^\phi\right]}{2\left[1 + cos\left(\frac{\phi\pi}{2}\right)\right]} \tag{45}$$

subtracting Eq. (31) from Eq. (44), determines the degree of "depression" of the semicircles and, in this case, the difference between the ideal and anomalous spectra. Logically, Eq. (44) (minus R_{dc}) and (45) provide the same result when $\phi = 1$ [18]. Furthermore, we note that, on the one hand, the high- and low-frequency limit of $Z_r(\omega)$ are $1/f'_V$ and $-g'_X/f'_X g'_V - g'_X f'_V$, respectively. On the other hand, $Z_j(\omega)$ tends to zero for both frequency regions. By substituting the numerical values used in the simulation of Fig. 3(c) in Eq. (45), it is possible to explain the differences in the imaginary part of the impedance at sufficiently low frequencies.

3. Negative spikes in dispersive transient currents

We next study the time transient response of the generalized model to a step perturbation, starting at V_0, of height ΔV:

$$v(t) = V_0 + \Delta V u(t) \tag{46}$$

which was studied in a previous publication by considering ideal conditions [16]. Note that $u(t)$ is the Heaviside step function (0 for $t < 0$ and 1 for $t > 0$). Remember not to confuse $v(t)$ (voltage at the terminals of the equivalent circuit) with $V(t)$ (voltage across the three-branched circuit). To analyze the transient dynamics at an equilibrium point, we consider that the increment ΔV represents a small change in the initial perturbation V_0 and thus, the systems under study can be analyzed, mathematically, from the linearized version of Eqs. (10)–(12) or, from an electrical point of view, by the equivalent circuit shown in Fig. 2 and previously analyzed in the frequency-domain. Generally, V_0 represents a constant high voltage value for stabilizing the electrical properties of the systems to a safe current value, $i_{total}(0^-)$, in the "inductive region" of the current-voltage characteristic. Therefore, Eq. (46) indicates that V_0 is applied for a "sufficiently long time" and, at the instant $t = 0$, voltage $v(t)$ is abruptly changed in equilibrium conditions. In the Appendix B, we derive the general properties of the characteristic parameters in this transient analysis.

Since fractional-order capacitor blocks dc current and dispersive inductor is considered to be discharged just after applying the voltage change (at the instant $t = 0$), $\Delta i_{total}(t)$ (or $i_{total}(t) - i_{total}(0^-)$) immediately starts a Mittag-Leffler decay, at extremely short time scales, from $i_{total}(0^+)$ toward a pseudo-constant value given by $\Delta V f'_V/(1 + R_s f'_V) \sim \Delta V f'_V$. Circuit theory [36] reveals that the fast decay process of $\Delta i_{total}(t)$ can be described according to the following relationship:

$$\Delta i_{total,ST}(t) = \Delta V f'_V + \frac{\Delta V}{R_s} E_\alpha\left[-\left(\frac{t}{\tau_{ST}}\right)^\alpha\right], \quad t \text{ comparable to } \tau_{ST} \tag{47}$$

where only the conductive line, in this short time scale, is "activated" in the equivalent circuit of Fig. 2(b). In effect, in the long term (that is, for $t \gg \tau_{ST}$), the current approaches an intermediate dc value, an "electrical manifestation" of the fact that the dispersive capacitance is fully charged and acts as an open circuit. Note that, by using the high-frequency impedance approximation of the circuit shown in Fig. 2, Eq. (47) can also be obtained by numerical inversion of the Laplace transform with $s \to \infty$. At the instant in which t and τ_{LT} are comparable in value, it starts an exponential rise toward a new steady state given by Eq. (B.3). Thus,

$$\Delta i_{total,LT}(t) = -\Delta V \frac{f'_X g'_V}{g'_X}\left(1 - \frac{g'_X f'_V}{f'_X g'_V} - E_\phi\left[-\left(\frac{t}{\tau_{LT}}\right)^\phi\right]\right), \quad t \text{ comparable to } \tau_{LT} \tag{48}$$

equivalent to $\mathscr{L}^{-1}\left[\Delta V Y(s)/s\right]$ considering the approximations previously mentioned, $s \to 0$. Assuming that $t \ll \tau_{LT}$ (short time scale of the governing transient term), the first two non-vanishing terms in the power series of the Mittag-Leffler function (refer to Eq. (24)) are considered: $E_\phi\left[-\left(t/\tau_{LT}\right)^\phi\right] = 1 - \left(t/\tau_{LT}\right)^\phi$. Eq. (48) is approximated by:

$$\Delta i_{total,LT}(t) = \Delta V\left(f'_V + f'_X g'_V t^\phi\right), \quad t \ll \tau_{LT} \tag{49}$$

which it follows that the portion of the transient response in this time window can be described in terms of an asymptotic power-law at the instant just after the trend change. From Eqs. (47) and (48), we can obtain a reasonable approximation of the overall transient response $\Delta i_{total}(t)$ due to the "small excursion" of voltage ΔV (see Eq. (46)):

$$\Delta i_{total}(t) = \frac{\Delta V}{R_s} E_\alpha\left[-\left(\frac{t}{\tau_{ST}}\right)^\alpha\right] - \Delta V \frac{f'_X g'_V}{g'_X}\left(1 - \frac{g'_X f'_V}{f'_X g'_V} - E_\phi\left[-\left(\frac{t}{\tau_{LT}}\right)^\phi\right]\right) \tag{50}$$

which is approximately equal to the result obtained from the following inverse Laplace transformation: $\mathscr{L}^{-1}\left[\Delta V Y(s)/s\right]$ [37]. In effect, the transient response to a change in the applied voltage, Eq. (46), at the input of the circuit shown in Fig. 2 has been obtained from the basic electrical laws. As it exits a mathematical connection between the time and frequency domain by the use of Laplace transform methods, the calculations can be also performed with the help of Eq. (29) and the corresponding approximations for the limiting cases of low and high frequency.

Eq. (65) allows one to go beyond the "simple" fractional kinetics. Fig. 4 illustrates the bifractional dynamics of $\Delta i_{total}(t)$ for different values of α and ϕ. Basically, the Mittag-Leffler function governs both time scales, exhibiting essentially faster decays as the fractional-order pattern decreases. In this transient analysis, note that we have only considered the case where the electrical parameters L_ϕ and R_a are positive and thus, the relaxation processes exhibit the ubiquitous negative spikes, widely visible in a multitude of experimental multidisciplinary situations [3,13,16]. Indeed, the rest of scenarios, previously studied in Section 2, exhibit classical patterns in the mathematically equivalent time-domain that have already been analyzed in the literature [38–40]. As can been seen in Fig. 4, the characteristic time scale of the negative spike components depends strongly on the fractional-order derivatives, requiring thus a robust mathematical background of such distributed relaxation processes to adequately estimate the temporal location of this
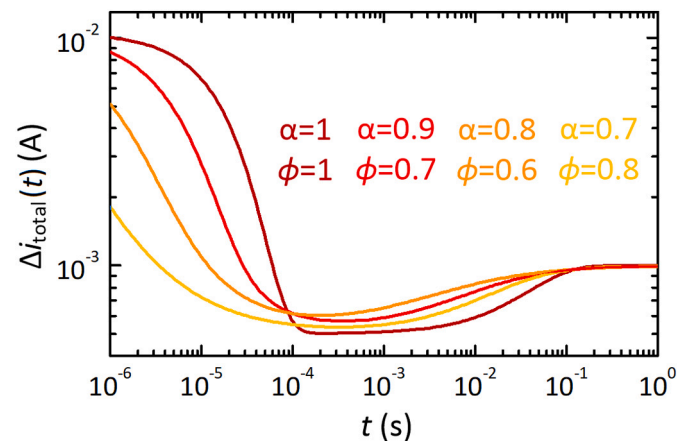

Fig. 4. Representations of negative spikes in current transient responses, as a function of α and ϕ. $R_s = 1\ \Omega$, $C_\alpha = 20\ \mu F\ s^{\alpha-1}$, $f'_V = 0.05\ \Omega^{-1}$, $g'_V = 1$, $f'_X = 1$, and $g'_x = -20\ s^{-1}$.

fundamental parameter.

In the following, we shall obtain the spike time and maximum negative overshoot of the general transient response given by Eq. (50). These values will be obtained in terms of the partial derivatives of Eqs. (15 and 16), and the parameters of the electrical circuits shown in Fig. 2. As previously indicated, the system is assumed to be "inductive" (refer to Fig. 3(a)). Before proceeding to determine such parameters, it is instructive to examine the asymptotic behavior of the Mittag-Leffler function. Negative spikes occurs when both $\Delta i_{\text{total,ST}}(t)$ and $\Delta i_{\text{total,LT}}(t)$ are approximately $\Delta V f'_V$, i.e., $t \gg \tau_{\text{ST}}$ and $t \ll \tau_{\text{LT}}$. At this time scale, the combination of two fractional processes with different characteristic time constants (refer to Eqs. (47), (48), and (50)) contains generalized relaxation functions in divergent stages of the strictly monotonically decreasing pattern. Specifically, $E_\alpha\left[-\left(t/\tau_{\text{ST}} \right)^\alpha \right]$ is about to disappear and $E_\phi\left[-\left(t/\tau_{\text{LT}} \right)^\phi \right]$ to emerge. Both Mittag-Leffler functions turn from initial stretched exponential behaviors (or truncated, after the second term, power series) to terminal inverse power-law patterns. We can therefore express $E_\alpha\left[-\left(t/\tau_{\text{ST}} \right)^\alpha \right]$ and $E_\phi\left[-\left(t/\tau_{\text{LT}} \right)^\phi \right]$, at the instant the current reaches the spike component, as [41,42]:

$$E_\alpha\left[-\left(\frac{t}{\tau_{\text{ST}}} \right)^\alpha \right] \sim \sum_{k=1}^{\infty} (-1)^{k-1} \frac{\left[-\left(t/\tau_{\text{ST}} \right)^\alpha \right]^{-k}}{\Gamma(1 - \alpha k)} \sim \frac{\left(t/\tau_{\text{ST}} \right)^{-\alpha}}{\Gamma(1 - \alpha)}, \quad t \gg \tau_{\text{ST}} \tag{51}$$

$$E_\phi\left[-\left(\frac{t}{\tau_{\text{LT}}} \right)^\phi \right] \sim exp\left[-\frac{\left(t/\tau_{\text{LT}} \right)^\phi}{\Gamma(\phi + 1)} \right] \sim \sum_{k=0}^{1} \frac{\left[-\left(t/\tau_{\text{LT}} \right)^\phi \right]^k}{\Gamma(\phi k + 1)}$$

$$= 1 - \frac{\left(t/\tau_{\text{LT}} \right)^\phi}{\Gamma(\phi + 1)}, \quad t \ll \tau_{\text{LT}} \tag{52}$$

by using the two common asymptotic approximations for the Mittag-Leffler function.

Referring to Eqs. (50), (51), and (52), we can obtain the spike time t_{spike} by differentiating $\Delta i_{\text{total}}(t)$ with respect to time, letting this derivative equal zero

$$\frac{d[\Delta i_{\text{total}}(t)]}{dt}\bigg|_{t=t_{\text{spike}}} = 0 \rightarrow -\alpha \frac{\Delta V}{R_s} \frac{\tau_{\text{ST}}^\alpha}{t_{\text{spike}}^{\alpha+1} \Gamma(1-\alpha)} - \phi \Delta V \frac{f'_X g'_V}{g'_X} \frac{t_{\text{spike}}^{\phi-1}}{\tau_{\text{LT}}^\phi \Gamma(\phi+1)} = 0 \tag{53}$$

and rearranging terms:

$$t_{\text{spike}} = \left[\frac{g'_X \tau_{\text{ST}}^\alpha \tau_{\text{LT}}^\phi \Gamma(\phi)}{f'_X g'_V R_s \Gamma(-\alpha)} \right]^{1/\alpha+\phi} \tag{54}$$

The maximum negative overshoot M_p occurs at the spike time t_{spike} [43]. As the final value of the current is $\Delta V\left(f'_V - f'_X g'_V / g'_X \right)^{-1}$ (see Eq. (B.3)), M_p can be thus calculated using the following equation:

$$M_p = \frac{\Delta i_{\text{total}}(t_{\text{spike}}) - \Delta i_{\text{total}}(\infty)}{\Delta i_{\text{total}}(\infty)} \times 100\% = \left(\frac{f'_X g'_V}{f'_V g'_X - f'_X g'_V} \right) \times 100\% \tag{55}$$

Eqs. (54) and (55) are obviously approximations but work well in the representative example shown in Fig. 4, obtaining spike times on the order of a few hundred milliseconds (0.31 ms for $\alpha = 0.9$ and $\phi = 0.7$; 0.17 ms for $\alpha = 0.8$ and $\phi = 0.6$; 0.31 ms for $\alpha = 0.7$ and $\phi = 0.8$) with the following magnitude of the minimum value, approximately measured from the steady-state value: -50%. Note that for $\alpha = 1$ and $\phi = 1$ (exponential relaxations in Eq. (50)), Eq. (54) becomes $t_{\text{spike}} = ln\left(R_s^2 C_\alpha f'_X g'_V \right) / \tau_{\text{LT}}^{-1} - \tau_{\text{ST}}^{-1}$ (0.22 ms in Fig. 4), maintaining Eq. (55)

invariable since it is independent of the fractional-order derivatives [16]. Finally, it should be mentioned that Eq. (54) must be used with care due to the asymptotic behavior and subsequent discontinuities of the Gamma function.

4. A note on the inverted hysteresis curves

In the following, we will briefly study the current in response to a voltage sweep at a constant velocity s (scan rate). Now, the voltage makes a large excursion of hundreds of mV, according to the following voltage dependence on time [44]:

$$V(t) = V_0 + st \tag{56}$$

which leads to a dynamic nonlinearity which manifests in the current-voltage curves obtained, in a wide variety of processes of different nature, through the technique of cyclic voltammetry [26,45].

It is common to obtain dramatic differences in the forward and reverse scans with significant resistive changes (hysteresis effects), depending on the previous history of the internal state variables of the system under scrutiny [44,46]. When the forward current is larger than in backward, this undesired effect is called capacitive or normal hysteresis. The vast majority of reports focus on this stereotypical current-voltage behavior. In this case, the capacitive-nature currents introduce the presence of additional contributions (positives in forward scanning and negatives in reserve direction) to the equilibrium current that modify the operating response of the system [47]. The dispersive and capacitive current $i_\alpha(V)$ increases proportionally to the scan rate following a power-law of the form [48,49]:

$$i_\alpha(V) = C_\alpha \frac{(V - V_0)^{1-\alpha}}{\Gamma(2 - \alpha)} s^\alpha \tag{57}$$

that produces a characteristic square loop with a slight surrounding in the edges. However, the opposite behavior of normal hysteresis is also observed in experimental measurements. It is clear that the origin behind of inverted hysteresis is the inductive effects, because makes emerge the feature of negative capacitance that changes the sign of the time transients at long time scales [50]. From Eqs. (10), (11), and (12), we can obtain the non-linear trend of the anomalous transient inductive currents [3] as:

$$i_x(V) = -\tau_L^\phi \frac{d^\phi X(t)}{dt^\phi} = -(\tau_L s)^\phi \frac{d^\phi X(t)}{dV^\phi} \tag{58}$$

which could explain the new kind of hysteretic distortion that arises mainly around high values at forward bias. As $d^\phi X(t)/dV^\phi > 0$ in a forward scanning, the additional current now is negative.

Here, we apply the general theory of the dispersive chemical inductor to current-voltage characteristics. We reformulate Eqs. (10), (11), and (12) as follows [46]:

$$C_\alpha \frac{d^\alpha V(t)}{dt^\alpha} = i_{\text{total}}(V) - i_x(t) \tag{59}$$

$$\tau_L^\phi \frac{d^\phi i_x(t)}{dt^\phi} = i_{a0} exp\left(\frac{V}{V_a} \right) + i_{b0} exp\left(\frac{V}{V_b} \right) - i_x(t) \tag{60}$$

where V_b and V_a are ideality factors defined, for practical reasons, in terms of voltage: $mk_B T/q$, with m as an ideality factor for each parameter, $k_B T$ as the thermal energy, and q as the elementary charge. Obviously, we can extract, from Eqs. (59) and (60), the stationary current:

$$i_{\text{total}}(V) = i_{a0} exp\left(\frac{V}{V_a} \right) + i_{b0} exp\left(\frac{V}{V_b} \right) \tag{61}$$

Specifically, Eqs. (59) and (60), for a voltage sweep measurement at a constant scan rate, become
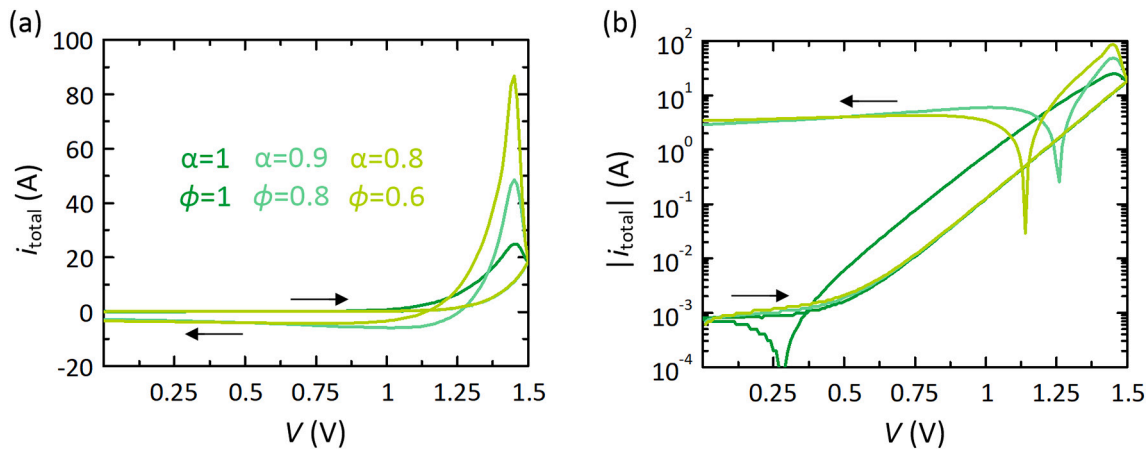
Fig. 5. Numerical simulations of current-voltage characteristics with a dispersive capacitance and a constant-phase inductive element in (a) linear and (b) logarithmic representation as a function of the fractional-order derivatives α and ϕ. Note that the absolute values of current are shown in (b). Parameters: $C_\alpha = 10$ mF s$^{\alpha-1}$, $i_{a0} = 10^{-7}$ A/$_{cm^2}$, $V_a = 0.2$ V, $i_{b0} = 10^{-5}$ A/$_{cm^2}$, $V_b = 0.1$ V, $\tau_L = 1$ s, and $s = 80$ mV/$_s$.

$$i_{\text{total}}(t) = C_\alpha \frac{\Delta V^{1-\alpha}}{\Gamma(2-\alpha)} s^\alpha + i_x(t) \tag{62}$$

$$V_R \frac{d^\phi i_x(t)}{dV^\phi} + i_x(t) - i_{a0} exp\left(\frac{V}{V_a}\right) - i_{b0} exp\left(\frac{V}{V_b}\right) = 0 \tag{63}$$

where, for convenience, we have redefined the sweep velocity parameter as:

$$V_R = s\tau_L \tag{64}$$

From the mathematical tools of fractional calculus, it is possible to solve the non-linear differential equation of fractional order of Eq. (63) and obtain numerical simulations of current-voltage curves (refer to Fig. 5) by using the non-integer-order derivative of Caputo [51]. In the ideal case ($\alpha = 1$ and $\phi = 1$) with an initial condition of $i_x(V_0) = i_{x0}$, we can easily obtain a "closed" analytical response of the slow internal stabilizing variable:

fractional-order capacitive currents on α parameter and scan rate values is available in the literature [39,40,48,49]. In the high-voltage region, inductive-based features emerge, causing negative transient currents that result in a highly ϕ-sensitive inverted hysteresis. To illustrate this point, consider what happens when ϕ value changes from 1 to 0.6, with a pseudo-constant α exponent, for a relatively fast forward and reverse voltage sweep (80 mV/s). The corresponding current-voltage curves are illustrated in Fig. 5. These summarized simulations show three fundamental regions: (i) non-ideal capacitive contributions dominating in the low voltage region –refer to Eq. (57)–; (ii) crossing points from regular to inverted hysteresis at intermediate values of V [53,54]; and (iii) at sufficiently high values of voltage, anomalous inductive-nature currents which, when ϕ parameter decreases, $i_x(V)$ theoretically exhibits slower continuous rises due to the Mittag-Leffler pattern, involving more prominent differences between the resulting current and the steady-state regime. This generalized model sheds light on the real operation and characteristics of a class of systems (that belong to a wide variety of research fields), leading to a more accurate analysis, than the classical

$$i_x(V) = \frac{V_a}{V_a + V_R} i_{a0} exp\left(\frac{V}{V_a}\right) + \frac{V_b}{V_b + V_R} i_{b0} exp\left(\frac{V}{V_b}\right) + \left(i_{x0} - \frac{V_a}{V_a + V_R} i_{a0} exp\left(\frac{V_0}{V_a}\right) - \frac{V_b}{V_b + V_R} i_{b0} exp\left(\frac{V_0}{V_b}\right)\right) exp\left(\frac{V_0 - V}{V_R}\right), \quad \alpha = 1, \phi = 1 \tag{65}$$

Under slow scan rates, $V_a > V_R$ and $V_b > V_R$, $i_x(V) \sim i_{a0} exp\left(V/_{V_a}\right) + i_{b0} exp\left(V/_{V_b}\right)$, and thus $i_{\text{total}}(V)$ will be approximately equal to the dc current that gives the steady-state values (see Eq. (61)). In this scenario, hysteresis effects will not appear when measuring the current-voltage curves. On the other hand, one obtains, in the first term on the right-hand side of Eq. (65), that $V_a < V_R$, $V_b < V_R$, and $i_x(V) \sim \left(V_a/_{V_R}\right) i_{a0} exp\left(V/_{V_a}\right) + \left(V_b/_{V_R}\right) i_{b0} exp\left(V/_{V_b}\right)$ under fast voltage sweeps, giving rise to hysteresis phenomena [46]. Note that the second term, that plays a relevant role at high scan rates, can be recognized as a transient current related to the initial conditions.

A further study of the dynamic current response indicates that, in "inductive hysteresis", $i_{\text{total}}(V)$ decreases as a power-law function of the driving scan rate, and not inversely proportional as when one considers an ideal chemical inductor, for the fractional-order model (Mittag-Leffler vs. exponential pattern [18,52]). As discussed previously, dispersive and capacitive hysteretic currents are clearly visible in the non-linear response at low voltages. Analysis of critical dependences of

studies, of the inverted hysteresis mechanisms obtained in experimental measurements.

5. Conclusions

We formulated a dynamical model for a common structure in a broad variety of materials and systems, in which anomalous inductive phenomena of chemical origin emerge as a consequence of slow ionic channels with fractional-order time-dependent dynamics. Our generalized analysis of two-dimensional fast-slow systems leads to a specific equivalent circuit that contains the duality of the famous CPE: the capacitive mode, that exists in practically all systems, and the fascinating pseudo-inductance feature, familiar in many research fields. In that regard, we summarized a visual map of very different spectral shapes displaying frequency dispersions in impedance tests, related to the inherent dynamical properties of the systems. This procedure is extended to study the associated regimes of time transients, exhibiting bifractional dynamics and the negative spike component, and the inverted hysteresis in current-voltage characteristics. Although the

consideration of constant-phase effects introduces a great deal of mathematical complexity in the analysis of experimental measurements, it also enables us to recognize the real dynamical properties of a wide range of material processes of different nature.

CRediT authorship contribution statement

All work in this single-author paper has been carried out by Enrique Hernández-Balaguera.

Compliance with ethics requirements

This article does not contain any studies with human or animal subjects.

Declaration of competing interest

The authors declare that they have no known competing interests or personal relationships that could have appeared to influence the work reported in this paper.

Data availability

Data will be made available on request.

Appendix A. Inductor theory from the perspective of the constant phase element (CPE)

From Eq. (4) where $Z_\phi(\omega) = V_\phi(\omega)/I_\phi(\omega)$, we can determine, as a representative example, the real and imaginary parts of the inductive-nature voltage:

$$V_\phi(\omega) = L_\phi(j\omega)^\phi I_\phi(\omega) = L_\phi\omega^\phi I_\phi(\omega)exp\left[j\frac{\phi\pi}{2}\right] = L_\phi\omega^\phi I_\phi(\omega)\left[cos\left(\frac{\phi\pi}{2}\right) + j\ sin\left(\frac{\phi\pi}{2}\right)\right] = L_\phi j\omega^\phi I_\phi(\omega)sin\left(\frac{\phi\pi}{2}\right)[1 - j\ tan(\theta)] \tag{A.1}$$

where

$$\theta = \frac{\pi(1-\phi)}{2} \tag{A.2}$$

which involves that the difference of phase, $-\phi\pi/2$, is constant and independent of frequency, as the name CPE already indicates. From a theoretical perspective, it is impossible to describe this "energy lost per cycle" (refer to Eq. (A.2)) by using an equivalent model with conventional passive components alone [55]. By separating the real and imaginary parts of the impedance in Eq. (4), it is possible, in this sense, to design a two-component model, consisting of a series resistor-inductor circuit:

$$Z_\phi(\omega) = R_{\text{eff}\phi}(\omega) + j\omega L_{\text{eff}\phi}(\omega) \tag{A.3}$$

with the following characteristic effective values:

$$R_{\text{eff}\phi}(\omega) = L_\phi\omega^\phi cos\left(\frac{\phi\pi}{2}\right) \tag{A.4}$$

$$L_{\text{eff}\phi}(\omega) = L_\phi\omega^{\phi-1}sin\left(\frac{\phi\pi}{2}\right) \tag{A.5}$$

and the associated time constant

$$\tau_{\text{eff}\phi}(\omega) = \omega^{-1}tan\left(\frac{\phi\pi}{2}\right) \tag{A.6}$$

which represents the internal operating space for the inductive model of the CPE. Note that $R_{\text{eff}\phi}(\omega)$ ($L_{\text{eff}\phi}(\omega)$ and $\tau_{\text{eff}\phi}(\omega)$) is frequency-dependent and theoretically found to increase approximatively in direct (inverse) proportion to ω. In the limit $\phi = 1$, both effective parameters associated to electrical components (Eqs. (A.4) and (A.5)), based on power-law patterns, reduce to the corresponding classical results (Eq. (3)) in frequency domain. In contrast, transient analysis stands out in that it does not contain, in some cases, the exponential relaxation function as a limiting case.

The charge distribution due to the presence of ionic-electronic effects in physical systems with anomalous interactions [56] and energetic inhomogeneities [32,57] generally involves analysis problems of a great complexity. For instance, the chemical inductor generates the feature of negative capacitance at low frequencies, which is fairly general in a wide variety of materials and systems [26,45]. This interesting phenomenon can be easily visualized from the experimental impedance data $Z(\omega)$ and the concept of complex capacitance, $C^*(\omega)$. Both functions are related by the following expression: $C^*(\omega) = 1/{j\omega Z(\omega)}$, where the real part, $C_{\text{eff}}(\omega) = Re[C^*(\omega)]$, represents the "effective capacitance". When the frequency-domain response in the fourth quadrant (inductive effects) occurs in the complex plane impedance plot, $C_{\text{eff}}(\omega)$ becomes negative. By Eq. (4), the effective capacitance of the dispersive inductor of chemical origin is [7]:

$$C_{\text{eff}\phi}(\omega) = -\frac{sin(\phi\pi/2)}{L_\phi\omega^{\phi+1}} \tag{A.7}$$

resulting in $C_{\text{effL}}(\omega) = -1/{L\omega^2}$ for the ideal case ($\phi = 1$, $L_\phi = L$) [3]. If one however considers an effective capacitance in Eq. (A.3) instead of the

chemical dispersive inductor, $Z_\phi(\omega) = R_{\mathrm{eff}\phi}(\omega) + 1/j\omega C_{\mathrm{eff}\phi}(\omega)$, $C_{\mathrm{eff}\phi}$ results in a different expression than that of Eq. (A.7). This disparity of expressions represents one of the most typical and significant problems, also observed in the constant-phase capacitive element, in the context of fractional dynamics and non-ideal relaxation processes.

Appendix B. Characteristic parameters in the time-domain charge of the dispersive inductor of chemical origin

A preceding dc steady-state value of $i_{\mathrm{total}}(t)$ is approached at time $t = 0^-$

$$i_{\mathrm{total}}(0^-) = V_0\left(f'_\mathrm{V} - \frac{f'_\mathrm{X} g'_\mathrm{V}}{g'_\mathrm{X}}\right)^{-1} \tag{B.1}$$

instant in which both versions of the CPE, capacitive and inductive, behave as an open- and a short-circuit, respectively: $i_{\mathrm{total}}(0^-) = V_0/R_{\mathrm{dc}}$ (initial condition). Remember that we consider series resistance effects to be negligible in comparison with the three-branched circuit. At time $t = 0$, the excitation is suddenly increased from V_0 to $V_0 + \Delta V$. Since the voltage across the constant-phase capacitive element cannot change instantaneously, i. e., $V(0^+) = V(0^-)$, the jump discontinuity of the current response at $t = 0$, is only due to the series resistance effects,

$$i_{\mathrm{total}}(0^+) - i_{\mathrm{total}}(0^-) = \frac{\Delta V}{R_\mathrm{s}} \tag{B.2}$$

and all the current flows through the dispersive capacitance in the two-branched region of circuit shown in Fig. 2(a). This result agrees with the fact that R_s is the limit of the impedance of Eq. (29) when $j\omega \to \infty$ (initial value theorem in Laplace domain): $\lim_{t\to 0} i_{\mathrm{total}}(t) = \lim_{s\to\infty} \Delta V Y(s)$. Just after, the current response decays, according to Eq. (47), and, beginning at the instant when the dispersive inductor of chemical origin emerges, the time transient starts to rise towards a new steady-state, which is mathematically expressed as:

$$\Delta i_{\mathrm{total}}(\infty) = \Delta V\left(f'_\mathrm{V} - \frac{f'_\mathrm{X} g'_\mathrm{V}}{g'_\mathrm{X}}\right)^{-1} \tag{B.3}$$

or $i_{\mathrm{total}}(\infty) = V_0 + \Delta V/R_{\mathrm{dc}}$, when, in practice, $t \gg \tau_{\mathrm{LT}}$. Again, Eq. (48) agrees with the results obtained using the final value theorem: $\lim_{t\to\infty} \Delta i_{\mathrm{total}}(t) = \lim_{s\to 0} \Delta V Y(s)$.

Indeed, admittance function $Y(s)$ exhibits a universal importance in current-voltage analysis because the characteristic or reference frequencies of the general response, i.e., the poles of the transfer function $I(s)/V(s)$,

$$\omega_{\mathrm{HF}} = \left(\frac{1 + R_\mathrm{s} f'_\mathrm{V}}{R_\mathrm{s} C_\alpha}\right)^{1/\alpha} \sim \left(\frac{1}{R_\mathrm{s} C_\alpha}\right)^{1/\alpha} \tag{B.4}$$

$$\omega_{\mathrm{LF}} = \left(\frac{R_\mathrm{s} f'_\mathrm{X} g'_\mathrm{V}}{R_\mathrm{s} f'_\mathrm{V} + 1} - g'_\mathrm{X}\right)^{1/\phi} \sim \left(-g'_\mathrm{X}\right)^{1/\phi} \tag{B.5}$$

are directly correlated with the time constants corresponding to the transient dynamic of the current $i_{\mathrm{total}}(t)$:

$$\tau_{\mathrm{ST}} = \left(R_\mathrm{s} C_\alpha\right)^{1/\alpha} \tag{B.6}$$

$$\tau_{\mathrm{LT}} = \left(-\frac{1}{g'_\mathrm{X}}\right)^{1/\phi} \tag{B.7}$$

that, as a unified property in systems that show this anomalous feature [27], involve strongly separated processes:

$$\tau_{\mathrm{LT}} \gg \tau_{\mathrm{ST}} \tag{B.8}$$

and thus, the combined relaxation process $i_{\mathrm{total}}(t)$ can be analyzed separately [58], being the slow one the dominant mechanism. Typically, $1/R_\mathrm{s} \gg f'_\mathrm{V}$ and $R_\mathrm{s} f'_\mathrm{X} g'_\mathrm{V}/R_\mathrm{s} f'_\mathrm{V} + 1 \ll |-g'_\mathrm{X}|$ because the series resistance tends to zero, $R_\mathrm{s} \to 0$ (see above); thus, the assumptions of Eqs. (B.4) and (B.5) are justified. Note that Eqs. (22) and (B.7) are equivalent. It is important to point out that time constants τ_{ST} and τ_{LT} could have been obtained by inspection of the electrical equivalent circuit shown in Fig. 2: By reducing voltage input to zero (a short-circuit connection), the resistance "seen", from the constant-phase capacitive (inductive) element is R_b in parallel with R_s (the parallel connection of R_b and R_s, in series with R_a) by considering the dispersive inductance discharged (fractional-order capacitor fully charged), i.e., open-circuits [16,39].

References

[1] Nilsson JW, Riedel SA. Electric circuits. Pearson; 2019.
[2] Chua L, Desoear OA, Kuh ES. Linear and nonlinear circuits. McGraw-Hill; 1987.
[3] Bisquert J, Guerrero A. Chemical inductor. J Am Chem Soc 2022;144(13): 5996–6009.
[4] Wang S, Zhang J, Gharbi O, Vivier V, Gao M, Orazem ME. Electrochemical impedance spectroscopy. Nat Rev Methods Primers 2021;1:1–21.

[5] Fouda ME, Elwakil AS, Radwan AG, Allagui A. Power and energy analysis of fractional-order electrical energy storage devices. Energy 2016;111:785–92.

[6] Berruet M, Pérez-Martínez JC, Romero B, Gonzales C, Al-Mayouf AM, Guerrero A, et al. Physical model for the current–voltage hysteresis and impedance of halide perovskite memristors. ACS Energy Lett 2022;7:1214–22.

[7] Hernández-Balaguera E, Arredondo B, Pereyra C, Lira-Cantú M. Parameterization of the apparent chemical inductance of metal halide perovskite solar cells exhibiting constant-phase-element behavior. J Power Sources 2023;560:232614.

[8] Brandstätter H, Hanzu I, Wilkening M. Myth and reality about the origin of inductive loops in impedance spectra of lithium-ion electrodes - a critical experimental approach. Electrochim Acta 2016;207:218–23.

[9] Koper MTM. Non-linear phenomena in electrochemical systems. J Chem Soc Faraday Trans 1998;94:1369–78.

[10] Shkirskiy V, King AD, Gharbi O, Volovitch P, Scully JR, Ogle K, Birbilis N. Revisiting the electrochemical impedance spectroscopy of magnesium with online inductively coupled plasma atomic emission spectroscopy. ChemPhysChem 2015;16(3):536–9.

[11] Cole KS, Baker RF. Longitudinal impedance of the squid giant axon. J Gen Physiol 1941;24:771–88.

[12] Hodgkin AL, Huxley AF. A quantitative description of membrane current and its application to conduction and excitation in nerve. J Physiol 1952;117:500–44.

[13] Klotz D. Negative capacitance or inductive loop? – a general assessment of a common low frequency impedance feature. Electrochem Commun 2019;98:58–62.

[14] Mora-Seró I, Bisquert J, Fabregat-Santiago F, Garcia-Belmonte G, Zoppi G, Durose K, et al. Implications of the negative capacitance observed at forward bias in nanocomposite and polycrystalline solar cells. Nano Lett 2006;6:640–50.

[15] Pivac I, Šimić B, Barbir F. Experimental diagnostics and modeling of inductive phenomena at low frequencies in impedance spectra of proton exchange membrane fuel cells. J Power Sources 2017;365:240–8.

[16] Hernández-Balaguera E, Bisquert J. Negative transient spikes in halide perovskites. ACS Energy Lett 2022;7:2602–10.

[17] Mainardi F. On some properties of the mittag-leffler function $E\alpha(-t\alpha)$, completely monotone for $t>0$ with $0<\alpha<1$. Discrete Continuous Dyn Syst B 2014;19:2267–78.

[18] Metzler R, Klafter J. From stretched exponential to inverse power-law: fractional dynamics, Cole-Cole relaxation processes, and beyond. J Non Cryst Solids 2002;305:81–7.

[19] Gateman SM, Gharbi O, Gomes de Melo H, Ngo K, Turmine M, Vivier V. On the use of a constant phase element (CPE) in electrochemistry. Curr Opin Electrochem 2022;36:101133.

[20] Jorcin J-B, Orazem ME, Pébère N, Tribollet B. CPE analysis by local electrochemical impedance spectroscopy. Electrochim Acta 2006;51:1473–9.

[21] Lasia A. The origin of the constant phase element. J Phys Chem Lett 2022;13:580–9.

[22] Pajkossy T. Impedance of rough capacitive electrodes. J Electroanal Chem 1994;364:111–25.

[23] Podlubny I. Fractional differential equations: an introduction to fractional derivatives, fractional differential equations, to methods of their solution and some of their applications. Academic Press; 1998.

[24] Scherer R, Kalla SL, Tang Y, Huang J. The Grünwald-letnikov method for fractional differential equations. Comput Math Appl 2011;62:902–17.

[25] Rudolf H. Applications of fractional calculus in physics. World Scientific; 2000.

[26] Vivier V, Orazem ME. Impedance analysis of electrochemical systems. Chem Rev 2022;122:11131–68.

[27] Bisquert J. Hopf bifurcations in electrochemical, neuronal, and semiconductor systems analysis by impedance spectroscopy. Appl Phys Rev 2022;9:011318.

[28] Bisquert J. Negative inductor effects in nonlinear two-dimensional systems: oscillatory neurons and memristors. Chem Phys Rev 2022;3(4):041305.

[29] Bisquert J. Electrical charge coupling dominates the hysteresis effect of halide perovskite devices. J Phys Chem Lett 2023;14:1014–21.

[30] Sadkowski A. Small signal (local) analysis of electrocatalytic reaction. Pole-zero approach. J Electroanal Chem 1999;465(2):119–28.

[31] Ebadi F, Taghavinia N, Mohammadpour R, Hagfeldt A, Tress W. Origin of apparent light-enhanced and negative capacitance in perovskite solar cells. Nat Commun 2019;10:1574.

[32] Hernández-Balaguera E, Romero B, Najafi M, Galagan Y. Analysis of light-enhanced capacitance dispersion in perovskite solar cells. Adv Mater Interfaces 2022;9(9):2102275.

[33] Hamill DC. Lumped equivalent circuits of magnetic components: the gyrator-capacitor approach. IEEE Trans Power Electron 1993;8:97–103.

[34] Said LA, Radwan AG, Madian AH, Soliman AM. Two-port two impedances fractional order oscillators. Microelectron J 2016;55:40–52.

[35] Zhang D, Allagui A, Elwakil AS, Yan Z, Lu H. Active circuit model of low-frequency behavior in perovskite solar cells. Org Electron 2020;85:105804.

[36] Kuo FF. Network analysis and synthesis. John Wiley & Sons; 1962.

[37] Moya AA. Identification of characteristic time constants in the initial dynamic response of electric double layer capacitors from high-frequency electrochemical impedance. J Power Sources 2018;397:124–33.

[38] Allagui A, Freeborn TJ, Elwakil AS, Fouda ME, Maundy BJ, Radwan AG, et al. Review of fractional-order electrical characterization of supercapacitors. J Power Sources 2018;400:457–67.

[39] Hernández-Balaguera E, Romero B, Arredondo B, del Pozo G, Najafi M, Galagan Y. The dominant role of memory-based capacitive hysteretic currents in operation of photovoltaic perovskites. Nano Energy 2020;78:105398.

[40] Hernandez-Balaguera E, Munoz-Díaz L, Pereyra C, Lira-Cantú M, Najafi M, Galagan Y. Universal control strategy for anomalous ionic-electronic phenomenology in perovskite solar cells efficiency measurements. Mater Today Energy 2022;27:101031.

[41] Erdélyi A. Higher transcendental functionsVol. 3. McGraw-Hill; 1955.

[42] Gorenflo R, Kilbas AA, Mainardi F, Rogosin SV. Mittag-leffler functions, related topics and applications. Springer-Verlag; 2014.

[43] Ogata K. Modern control engineering. Prentice Hall; 2010.

[44] Bisquert J, Guerrero A, Gonzales C. Theory of hysteresis in halide perovskites by integration of the equivalent circuit. ACS Phys Chem Au 2021;1:25–44.

[45] Guerrero A, Bisquert J, Garcia-Belmonte G. Impedance spectroscopy of metal halide perovskite solar cells from the perspective of equivalent circuits. Chem Rev 2021;121:14430–84.

[46] Gonzales C, Guerrero A, Bisquert J. Transition from capacitive to inductive hysteresis: a neuron-style model to correlate I-V curves to impedances of metal halide perovskites. J Phys Chem C 2022;126:13560–78.

[47] Almora O, Zarazua I, Mas-Marza E, Mora-Sero I, Bisquert J, Garcia-Belmonte G. Capacitive dark currents, hysteresis, and electrode polarization in lead halide perovskite solar cells. J Phys Chem Lett 2015;6:1645–52.

[48] Hernández-Balaguera E, Arredondo B, del Pozo G, Romero B. Exploring the impact of fractional-order capacitive behavior on the hysteresis effects of perovskite solar cells: a theoretical perspective. Commun Nonlinear Sci Numer Simul 2020;90:105371.

[49] Hernández-Balaguera E, del Pozo G, Arredondo B, Romero B, Pereyra C, Xie H, et al. Unraveling the key relationship between perovskite capacitive memory, long timescale cooperative relaxation phenomena, and anomalous J-V hysteresis. Solar RRL 2021;5:2000707.

[50] Alvarez AO, Arcas R, Aranda CA, Bethencourt L, Mas-Marza E, Saliba M, et al. Negative capacitance and inverted hysteresis: matching features in perovskite solar cells. J Phys Chem Lett 2020;11:8417–23.

[51] Garrappa R. Predictor-corrector PECE method for fractional differential equations. MATLAB Central File Exchange, https://es.mathworks.com/matlabcentral/fil eexchange/32918-predictor-corrector-pece-method-for-fractional-differential-equations. [Accessed 26 February 2023].

[52] Gómez-Aguilar JF, Atangana A. New insight in fractional differentiation: power, exponential decay and mittag-leffler laws and applications. Eur Phys J Plus 2017;132:13.

[53] Filipoiu N, Preda AT, Anghel D-V, Patru R, Brophy RE, Kateb M, et al. Capacitive and inductive effects in perovskite solar cells: the different roles of ionic current and ionic charge accumulation. Phys Rev Appl 2022;18:064087.

[54] Nemnes GA, Besleaga C, Stancu V, Dogaru DE, Leonat LN, Pintilie L, et al. Normal and inverted hysteresis in perovskite solar cells. J Phys Chem C 2017;121:11207–14.

[55] Westerlund S, Ekstam L. Capacitor theory. IEEE Trans Dielectr Electr Insul 1994;1:826–39.

[56] Metzler R, Klafter J. The random walk's guide to anomalous diffusion: a fractional dynamics approach. Phys Rep 2000;339:1–77.

[57] Córdoba-Torres P, Mesquita TJ, Nogueira RP. Relationship between the origin of constant-phase element behavior in electrochemical impedance spectroscopy and electrode surface structure. J Phys Chem C 2015;119:4136–47.

[58] Gómez-Aguilar JF, Yépez-Martínez H, Escobar-Jiménez RF, Astorga-Zaragoza CM, Reyes-Reyes J. Analytical and numerical solutions of electrical circuits described by fractional derivatives. App Math Model 2016;40:9079–94.